AIAA JOURNAL
Vol. 45, No. 3, March 2007

Optimality Conditions of the Hybrid Cellular Automata for Structural Optimization

Andrés Tovar*
National University of Colombia, Carrera 30 45-03, Bogotá, Colombia
and
Neal M. Patel,† Amit K. Kaushik,‡ and John E. Renaud§
University of Notre Dame, Notre Dame, Indiana 46556

DOI: 10.2514/1.20184

The hybrid cellular automaton method has been successfully applied to topology optimization using a uniform strain energy density distribution approach. In this work, a new set of design rules is derived from the first-order optimality conditions of a multi-objective problem. In this new formulation, the final topology is derived to minimize both mass and strain energy. In the hybrid cellular automaton algorithm, local design rules based on the cellular automaton paradigm are used to efficiently drive the design to optimality. In addition to the control-based techniques previously introduced, a new ratio technique is derived in this investigation. This work also compares the performance of the control strategies and the ratio technique.

Nomenclature

c_D	=	derivative control gain
c_I	=	integral control gain
c_P	=	proportional control gain
c_T	=	two-position control gain
$\boldsymbol{d}$	=	nodal displacement vector
E	=	Young's modulus
$\boldsymbol{f}$	=	nodal force vector
$\mathbf{k}$	=	stiffness matrix
$\mathcal{L}$	=	Lagrangian function
M	=	mass of the structure
m	=	mass of an element
N	=	number of cells in the design domain
$\hat{N}$	=	number of neighbors of a cell
p	=	penalization power
$\boldsymbol{R}$	=	evolutionary rules
t	=	discrete time
U	=	strain energy
u	=	strain energy density
v	=	volume of an element
x	=	design variable
y	=	state variable
$\boldsymbol{\alpha}$	=	cell state
ε	=	tolerance for convergence
$\boldsymbol{\lambda}$	=	Lagrange multipliers
ν	=	Poisson's ratio
ρ	=	density
τ	=	dummy time variable
ω	=	weight coefficient

Subscripts

i	=	refers to the element or cell
k	=	refers to the neighboring cell
0	=	refers to the base, solid material

Superscripts

T	=	transpose operator
*	=	refers to an optimum value

I. Introduction

TOPOLOGY optimization involves the optimal distribution of material within a design domain. Initially, the design domain comprises a large number of elements. The topology optimization process finds an optimal structure by selectively removing unnecessary elements from the design domain. The design variables in the optimization problem depend on the type of material model used in the structural analysis. The most commonly referenced approaches are the homogenization model [1–3] and the solid isotropic material with penalization (SIMP) model [4–6].

In topology optimization, the number of elements and, hence, the number of design variables depends on the size of the design domain and the desired resolution of the final structure. Even the design of a small mechanical component might involve thousands of design variables. In addition, the cost of a function call increases with the number of elements. Therefore, the use of classical gradient-based optimization methods might be impractical. This has motivated the implementation of specialized numerical methods such as approximation techniques [7–9], methods of moving asymptotes (MMA) [10], optimality criteria [11–13], genetic algorithms [14,15], the so-called evolutionary structural optimization (ESO) approach [16,17], and cellular automaton (CA) techniques [18–23].

A basic CA-like approach was developed by Inou et al. [24]. In their approach, the elastic moduli of the cells are used as the design variables. A local rule iteratively updates the value of the modulus of each cell based on the difference between a current stress value and a target value. Evolutionary rules based on the growing/reforming procedure are used to fine-tune the structure. Cells with low elastic modulus are removed, while cells with high elastic modulus create a new cell in an empty surrounding space. This approach led to

Presented as Paper 1898 at the 46th AIAA/ASME/ASCE/AHS/ASC Structures, Structural Dynamics and Materials Conference 13th AIAA/ASME/AHS Adaptive Structures Conference, Austin, Texas, 18–21 April 2005; received 22 September 2005; revision received 30 October 2006; accepted for publication 31 October 2006.

*Associate Professor, Department of Mechanical and Mechatronic Engineering; atovarp@unal.edu.co. Member AIAA.
†Graduate Research Assistant, Department of Aerospace and Mechanical Engineering; npatel@nd.edu. Student Member AIAA.
‡Research Assistant, Department of Aerospace and Mechanical Engineering; akaushik@nd.edu.
§Professor, Department of Aerospace and Mechanical Engineering; jrenaud@nd.edu. Associate Fellow AIAA.

structures that are similar to the ones observed in bird bones [18]. Even though this is not necessarily a topology optimization algorithm, it illustrates the application of an evolutionary CA model.

More recently, the concept of a CA model for topology optimization was presented by Kita and Toyoda [19]. In their approach, thickness is used as the design variable. The local design rule is derived from the optimality condition of a multi-objective function, in which both the weight of the structure and the deviation between the yield stress and the equivalent stress in a Moore neighborhood are to be minimized. The finite element method is used to evaluate the stress for each iteration. The algorithm requires hundreds of iterations to achieve convergence even in simple test problems.

The CA model presented by Tatting and Gürdal [20] is implemented with a simultaneous analysis and design (SAND) approach. In their work, both design and state variables are simultaneously updated. In their SAND-CA method, the use of local equilibrium equations eliminates the need for finite element analysis. While structural analysis is performed, local state variables are driven to target values. In this way, the residual between the work of internal and external forces is iteratively reduced to zero. Hundreds of thousands of iterations are required to achieve convergence; however, the overall computational time can be reduced compared to techniques based on the finite element method [25]. In the SAND-CA approach, the convergence can deteriorate as the number of elements increases. This occurs because the field variable information propagates slowly. Convergence difficulties for this CA-based approach have been studied by Slotta et al. [26] and Missoum et al. [27]. Multigrid and full multigrid acceleration strategies have shown to mitigate this problem [28]. In a recent publication, Abdalla and Gürdal [22] demonstrate the SAND-CA approach in application to the column design for buckling.

A different approach presented by Hajela and Kim [21] combines genetic algorithms (GAs) and cellular automata (CAs) for structural analysis of two-dimensional elastic problems. The local rules are derived using a GA optimization process and the principle of minimum energy. The strain fields exhibited in their results are very close to the ones obtained from the analytical solutions. Even though the CA method was not used for structural synthesis, their work shows a strategy to develop local rules for structural analysis and avoid the use of global analysis, that is, the finite element method.

The methodology developed in this research is referred to as a hybrid cellular automaton (HCA) algorithm. In conventional CA methods, a global analysis of field states is not performed. In this research, the HCA method makes use of the finite element analysis to evaluate the field states, that is, the strain energy densities. In this context, the work of Kita and Toyoda [19] can be considered a hybrid method because they use finite element analysis to update the stress states during each iteration of their algorithm. The HCA method is a finite element-based approach and, therefore, it reduces the residual between external work and internal energy to zero at every iteration. Conversely, in the SAND-CA implementation of Tatting and Gürdal [20], the residuals are iteratively reduced to zero by the analysis and design rules.

In Tovar et al. [23] a new approach to topology optimization was developed. This approach reduces numerical instabilities by using CA principles, as opposed to filtering techniques as used in [29]. This method is referred to as a HCA method with local control rules. In this approach, the design domain is discretized into a regular lattice of CAs. Each CA locally modifies the design variables according to a design rule. This rule drives the local strain energy density (SED) to a local SED target using a control strategy.

In this investigation, a new set of HCA design rules is derived from the Karush–Kuhn–Tucker (KKT) optimality conditions of a multi-objective problem. In this formulation, the design process seeks to minimize both mass and strain energy. In addition to the control-based techniques previously introduced, this work derives a new ratio technique that drives the design to optimality. This ratio technique is based on the one traditionally used to design truss structures in the fully stressed design (FSD) approach.

II. Material Model

The initial work in topology optimization was based on the design of continuum structures using microstructural geometrical characteristics as design variables. This technique, presented by Bendsøe and Kikuchi [1], is referred to as the homogenization approach. In this approach, the finite elements of the structure are made of a composite material consisting of an infinite number of infinitely small holes periodically distributed throughout a solid base. The topology optimization problem is transformed into a parameter optimization problem where the design variables are the material densities of the finite elements [30].

The density approach was later formalized by Bendsøe [4]. In this approach, the material distribution problem is parameterized by the elastic modulus E_i of the discrete isotropic finite elements. This approach requires the optimum structure to be a design consisting of regions with material, $E_i = E_0$, and regions without material, $E_i = 0$. E_0 is the elastic modulus of the isotropic base material. In this sense, the optimal topologies, based on the use of isotropic materials, rely on the family of the so-called black and white structures. Intermediate values for the elastic modulus (gray colors) have to be penalized. One of the most efficient techniques to achieve this condition is the so-called penalized proportional stiffness model or SIMP model [6]. This model is based on the heuristic relationship

$$E_i(x_i) = x_i^p E_0 \qquad (p > 1) \tag{1}$$

$$\rho_i(x_i) = x_i \rho_0 \qquad (0 \le x_i \le 1) \tag{2}$$

where ρ_0 is the density of the solid material, and ρ_i is a variable density [30]. The design variable in this approach is the relative density x_i. The power p is used to penalize intermediate relative density values and drive the design to a black and white structure. According to Bendsøe and Sigmund [31], the SIMP model can be considered as a material model if the power p satisfies the conditions

$$p \ge \max\left\{\frac{2}{1-\nu_0}, \frac{4}{1+\nu_0}\right\} \qquad \text{(in 2-D)} \tag{3}$$

$$p \ge \max\left\{15\frac{1-\nu_0}{7-5\nu_0}, \frac{3(1-\nu_0)}{2(1-2\nu_0)}\right\} \qquad \text{(in 3-D)} \tag{4}$$

where ν_0 is the Poisson's ratio of the given base material. From Eq. (3), a value of $\nu_0 = 0.3$ yields $p \ge \max\{2.857, 3.077\}$ in 2-D and $p \ge \max\{1.909, 2.625\}$ in 3-D. The violation of these conditions implies that the SIMP model cannot be considered a material model.

III. Optimization Problem

Let the optimum structure be of maximum stiffness and minimum weight. This condition can be expressed as a multi-objective optimization problem in which stiffness and mass are conflicting functions. Maximizing stiffness is equivalent to minimizing the strain energy. Following the procedure used by Saxena and Ananthasuresh [13], the multi-objective optimization problem can be stated as

$$\min_{\boldsymbol{x}} \quad c(\boldsymbol{x}) = f(U) + g(M) \qquad \text{s.t.} \quad \mathbf{0} \le \boldsymbol{x} \le \mathbf{1} \tag{5}$$

where $f(U)$ is a function of the strain energy and $g(M)$ is a function of the mass. As described by Eq. (2), the relative density x_i is defined by the ratio between ρ_0 and ρ_i. This can be expressed as

$$x_i = \frac{\rho_i}{\rho_0} \tag{6}$$

which varies between the limits 0 and 1. In practice, the lower boundary of x_i is not zero but a small positive value; for example, $x_{\min} = 1 \times 10^{-3}$. This condition guards against the singularity of the stiffness matrix during the application of the standard finite element analysis (FEA) [32,33],

$$\mathbf{k}\,\boldsymbol{d} - \boldsymbol{f} = \mathbf{0} \tag{7}$$

where $\mathbf{k}$ is the global stiffness matrix, $\boldsymbol{d}$ is the global nodal displacement vector, and $\boldsymbol{f}$ is the global equivalent nodal force vector.

If the structure is discretized into N elements, the internal energy or strain energy stored in the domain, U, can be approximated as

$$U = \frac{1}{2}\boldsymbol{d}^T\mathbf{k}\boldsymbol{d} = \frac{1}{2}\sum_{i=1}^{N}\boldsymbol{d}_i^T\mathbf{k}_i\boldsymbol{d}_i \tag{8}$$

and the total mass M is given by

$$M = \sum_{i=1}^{N} m_i = \sum_{i=1}^{N} x_i m_0 \tag{9}$$

where m_i is the variable mass of an element, and m_0 is the maximum mass of the element. Note that $m_0 = \rho_0 v_0$ and $m_i = \rho_i v_0$, where v_0 represents the volume of an element. Because v_0 is a constant value, then $m_i = x_i m_0$. For this reason, x_i is also referred to as the relative mass.

The Lagrangian of Eq. (5) is given by

$$\mathcal{L} = f(U) + g(M) + \boldsymbol{\lambda}_1^T(\boldsymbol{x} - 1) - \boldsymbol{\lambda}_0^T\boldsymbol{x} \tag{10}$$

where $\boldsymbol{\lambda}_0$ and $\boldsymbol{\lambda}_1$ are the Lagrangian multiplier vectors associated with the inequality constraints. The optimality conditions, or KKT conditions, of Eq. (5) are given by

$$\frac{\partial\mathcal{L}}{\partial x_i} = \frac{\partial f(U)}{\partial U}\frac{\partial U}{\partial x_i} + \frac{\partial g(M)}{\partial M}\frac{\partial M}{\partial x_i} + \lambda_{1i} - \lambda_{0i} = 0 \tag{11}$$

and

$$\lambda_{1i} \geq 0 \tag{12}$$

$$\lambda_{0i} \geq 0 \tag{13}$$

$$\lambda_{1i}(x_i - 1) = 0 \tag{14}$$

$$\lambda_{0i}x_i = 0 \tag{15}$$

For an interior point, $0 < x_i < 1$, Eqs. (12–15) are satisfied since $\lambda_{1i} = \lambda_{0i} = 0$. Therefore, the optimality condition in Eq. (11) is satisfied when

$$\frac{\partial f(U)}{\partial U}\frac{\partial U}{\partial x_i} + \frac{\partial g(M)}{\partial M}\frac{\partial M}{\partial x_i} = 0 \tag{16}$$

This optimality condition yields

$$\frac{\partial U/\partial x_i}{\partial M/\partial x_i} = -\frac{\partial g(M)/\partial M}{\partial f(U)/\partial U} \tag{17}$$

Using Eq. (8), the numerator of Eq. (17) can be expressed as

$$\frac{\partial U}{\partial x_i} = \frac{1}{2}\left(\frac{\partial \boldsymbol{d}^T}{\partial x_i}\mathbf{k}\boldsymbol{d} + \boldsymbol{d}^T\frac{\partial(\mathbf{k}\boldsymbol{d})}{\partial x_i}\right) \tag{18}$$

From Eq. (7) and taking into account that external forces $\boldsymbol{f}$ are independent of x_i, then

$$\frac{\partial(\mathbf{k}\boldsymbol{d})}{\partial x_i} = 0 \tag{19}$$

Therefore, Eq. (18) can be simplified to

$$\frac{\partial U}{\partial x_i} = \frac{1}{2}\frac{\partial \boldsymbol{d}^T}{\partial x_i}\mathbf{k}\boldsymbol{d} \tag{20}$$

Because the stiffness matrix $\mathbf{k}$ is symmetric, then

$$(\mathbf{k}\boldsymbol{d})^T = \boldsymbol{d}^T\mathbf{k} \tag{21}$$

Combining Eq. (21) with Eq. (19) yields

$$\frac{\partial(\mathbf{k}\boldsymbol{d})^T}{\partial x_i} = \frac{\partial(\boldsymbol{d}^T\mathbf{k})}{\partial x_i} = \frac{\partial \boldsymbol{d}^T}{\partial x_i}\mathbf{k} + \boldsymbol{d}^T\frac{\partial \mathbf{k}}{\partial x_i} = 0 \tag{22}$$

therefore,

$$\frac{\partial \boldsymbol{d}^T}{\partial x_i}\mathbf{k} = -\boldsymbol{d}^T\frac{\partial \mathbf{k}}{\partial x_i} \tag{23}$$

Substituting Eq. (23) into Eq. (20), one obtains

$$\frac{\partial U}{\partial x_i} = -\frac{1}{2}\boldsymbol{d}^T\frac{\partial \mathbf{k}}{\partial x_i}\boldsymbol{d} \tag{24}$$

Each term x_i is present only in its corresponding element stiffness matrix $\mathbf{k}_i$; therefore,

$$\frac{\partial \mathbf{k}}{\partial x_i} = \frac{\partial \mathbf{k}_i}{\partial x_i} \tag{25}$$

Using the active components of the nodal displacement vector $\boldsymbol{d}$, Eq. (24) can be expressed as

$$\frac{\partial U}{\partial x_i} = -\frac{1}{2}\boldsymbol{d}_i^T\frac{\partial \mathbf{k}_i}{\partial x_i}\boldsymbol{d}_i \tag{26}$$

Making use of the isotropic material model described by Eq. (1) yields

$$\mathbf{k}_i = \mathbf{k}_0 x_i^p \tag{27}$$

where $\mathbf{k}_0$ corresponds to the elastic stiffness matrix of the solid element. Deriving Eq. (27) with respect to x_i, one obtains

$$\frac{\partial \mathbf{k}_i}{\partial x_i} = p\mathbf{k}_0 x_i^{p-1} \tag{28}$$

Substituting Eq. (28) in Eq. (26) yields

$$\frac{\partial U}{\partial x_i} = -\frac{1}{2}\boldsymbol{d}_i^T p\mathbf{k}_0 x_i^{p-1}\boldsymbol{d}_i \tag{29}$$

If the strain energy density of the ith element, u_i, is expressed as

$$u_i = \frac{1}{2v_0}\boldsymbol{d}_i^T\mathbf{k}_0 x_i^p\boldsymbol{d}_i \tag{30}$$

then Eq. (29) can be finally written as

$$\frac{\partial U}{\partial x_i} = -pv_0\frac{u_i}{x_i} \tag{31}$$

On the other hand, making use of Eq. (9), the denominator of Eq. (17) can be expressed as

$$\frac{\partial M}{\partial x_i} = m_0 \tag{32}$$

where m_0 is the mass of a solid element. Finally, substituting Eqs. (31) and (32) into Eq. (17), the optimality condition can be expressed as

$$\frac{\partial U/\partial x_i}{\partial M/\partial x_i} = -\frac{pv_0}{m_0}\frac{u_i}{x_i} = -\frac{\partial g(M)/\partial M}{\partial f(U)/\partial U} \tag{33}$$

A conventional way to define $f(U)$ and $g(M)$ in Eq. (5) is as follows:

$$f(U) = \omega\frac{U}{U_0} \tag{34}$$

and

$$g(U) = (1-\omega)\frac{M}{M_0} \tag{35}$$

where U_0 and M_0, respectively, represent the strain energy and mass of the solid design domain. The coefficient ω balances the relative weight of the ratios U/U_0 and M/M_0 in the objective function, such that $0 \leq \omega \leq 1$. In this way, the optimality condition described by Eq. (33) can be written as

$$\frac{p}{\rho_0}\frac{u_i}{x_i} = \frac{(1-\omega)}{\omega}\frac{U_0}{M_0} \tag{36}$$

where the density of a solid element is given by $\rho_0 = m_0/v_0$. If one defines the state variable y_i as

$$y_i = \frac{u_i}{x_i} \tag{37}$$

where u_i is defined by Eq. (30), and its optimum value y_i^* as

$$y_i^* = \frac{u_i^*}{x_i^*} = \frac{(1-\omega)}{\omega}\frac{\rho_0}{p}\frac{U_0}{M_0} \tag{38}$$

then the optimality condition for an interior point can be simplified as

$$y_i = y_i^* \tag{39}$$

If the relative mass x_i of a discrete element is saturated, that is $x_i = 0$ or $x_i = 1$, then the optimality criteria defined in Eq. (39) no longer applies. If $x_i = 0$, then $\lambda_{1i} = 0$ and Eqs. (12), (14), and (15) are satisfied. Combining Eqs. (11) and (13), the remaining optimality conditions can be expressed as

$$\lambda_{0i} = \frac{\partial f(U)}{\partial U}\frac{\partial U}{\partial x_i} + \frac{\partial g(M)}{\partial M}\frac{\partial M}{\partial x_i} \geq 0 \tag{40}$$

Using the results from Eqs. (31) and (32), along with the assumption that $f(U) = \omega U$ and $g(M) = (1-\omega)M$, the Lagrange multiplier λ_{0i} can be defined as

$$\lambda_{0i} = -pv_0\frac{\omega}{U_0}\frac{u_i}{x_i} + m_0\frac{(1-\omega)}{M_0} \geq 0 \tag{41}$$

Organizing terms in Eq. (41) and using the definitions stated in Eqs. (37) and (38), the optimality condition for $x_i = 0$ can be expressed as

$$y_i \leq y_i^* \tag{42}$$

Now, if $x_i = 1$, then $\lambda_{0i} = 0$ and Eqs. (13–15) are satisfied. Combining Eqs. (11) and (12), the remaining optimality conditions can be expressed as

$$\lambda_{1i} = -\frac{\partial f(U)}{\partial U}\frac{\partial U}{\partial x_i} - \frac{\partial g(M)}{\partial M}\frac{\partial M}{\partial x_i} \geq 0 \tag{43}$$

Simplifying as before, Eq. (43) can be written as

$$\lambda_{1i} = pv_0\frac{\omega}{U_0}\frac{u_i}{x_i} - m_0\frac{(1-\omega)}{M_0} \geq 0 \tag{44}$$

Organizing terms, the optimality condition when $x_i = 1$ can be expressed as

$$y_i \geq y_i^* \tag{45}$$

In summary, one observes that $y_i = y_i^*$ for $0 < x_i < 1$, $y_i < y_i^*$ when $x_i = 0$, and $y_i > y_i^*$ when $x_i = 1$. The following task is to develop a local evolutionary rule that drives each element to a point where these optimality conditions are satisfied.

IV. Local Evolutionary Rule

This section presents two approaches to derive an evolutionary rule that drives the structure to the optimum configuration described by Eqs. (39), (42), and (45). These approaches are referred to as the *ratio technique* and the *control strategies*.

A. Ratio Technique

The problem presented above shares similarities with the FSD formulation which has been traditionally used to design truss structures. A FSD formulation states that "*For the optimum design each member of the structure that is not at its minimum gage is fully stressed under at least one of the design load conditions*" [34]. The technique that has been traditionally used to resize the truss elements in the structure is referred to as the ratio technique. Using the principle of the ratio technique, this research develops a new approach suitable for structures in a continuum.

Using Eq. (30), the state variable y_i, described by Eq. (46), can be expressed as

$$y_i = \frac{u_i}{x_i} = \frac{1}{2v_0}\frac{x_i^p}{x_i}\boldsymbol{d}_i^T\mathbf{k}_0\boldsymbol{d}_i \tag{46}$$

Its optimum value, y_i^*, defined by Eq. (38), can be expressed as the ratio between an optimum value of strain energy u_i^* and an optimum value of relative density x_i^* [35]. This is

$$y_i^* = \frac{u_i^*}{x_i^*} = \frac{1}{2v_0}\frac{x_i^{*p}}{x_i^*}\boldsymbol{d}_i^{*T}\mathbf{k}_0\boldsymbol{d}_i^* \tag{47}$$

where $\boldsymbol{d}_i^*$ is the nodal displacement vector of an element that satisfies the optimality conditions. Combining Eqs. (46) and (47), the ratio y_i^*/y_i can be stated as

$$\frac{y_i^*}{y_i} = \frac{x_i^{*p-1}}{x_i^{p-1}}\frac{\boldsymbol{d}_i^{*T}\mathbf{k}_0\boldsymbol{d}_i^*}{\boldsymbol{d}_i^T\mathbf{k}_0\boldsymbol{d}_i} \tag{48}$$

For small displacements, this fraction can be approximated to

$$\frac{y_i^*}{y_i} = \frac{x_i^{*p-1}}{x_i^{p-1}} \tag{49}$$

Solving for x_i^* yields

$$x_i^* = x_i\left(\frac{y_i^*}{y_i}\right)^{\frac{1}{p-1}} \tag{50}$$

Using Eq. (50), the updating rule can be written as

$$x_i(t+1) = x_i(t)\left(\frac{y_i^*}{y_i}\right)^{\frac{1}{p-1}} \tag{51}$$

where t is a discrete time step and $p > 1$. The power p is used to penalize intermediate relative density values and drive the design to a black and white structure. This work makes use of $p = 3$ for a two-dimensional structure; see Eq. (3).

B. Control Strategies

This approach is inspired by control models proposed in bone remodeling simulations [36–38]. The objective of a controller is to find the optimum values of the design variable x_i^* in order to drive an error function to zero. To solve the problem stated by Eqs. (39), (42), and (45), let us define the error function as

$$e_i(t) = y_i(t) - y_i^* \tag{52}$$

In control theory, the simplest strategy is the two-position control [39]. Using this controller, the change in mass is a piecewise constant function that can be expressed as

$$\frac{\mathrm{d}x_i(t)}{\mathrm{d}t} = \begin{cases} +c_T^F & \text{if } e_i(t) > 0 \\ 0 & \text{if } e_i(t) = 0 \\ -c_T^R & \text{if } e_i(t) < 0 \end{cases} \tag{53}$$

where c_T^F and c_T^R are positive constants. The superscripts F and R refer to the processes of formation and resorption. With the two-position control strategy, the net change in relative density is $+c_T^F$ if $y_i(t) > y_i^*$, and $-c_T^R$ if $y_i(t) < y_i^*$.

A more complex strategy makes use of the proportional-integral-derivative (PID) control. With the PID controller, the change in mass can be expressed as

$$\frac{\mathrm{d}x_i(t)}{\mathrm{d}t} = c_P e_i(t) + c_I \int_0^t e_i(\tau)\,\mathrm{d}\tau + c_D \frac{\mathrm{d}e_i(t)}{\mathrm{d}t} \tag{54}$$

where c_P, c_I, and c_D are positive constants, respectively, referred to as proportional, integral, and derivative gains. These evolutionary rules are now implemented into the hybrid cellular automaton algorithm.

The application of the local evolutionary rule (ratio technique and control strategy) has to consider the upper and lower boundaries of the design variables, that is, $x_{\min} \le x_i \le 1$. As explained before, the use of $x_{\min} = 1 \times 10^{-3}$ guards against the singularity of the stiffness matrix during the application of the standard finite element analysis. If after the application of the evolutionary rule x_i violates one of its boundaries, $x_i < x_{\min}$ or $x_i > 1$, the optimizer corrects it by setting the design variable value to its boundary.

V. Hybrid Cellular Automata

The time evolution of physical quantities is often governed by nonlinear partial differential equations. In many cases, the solutions of these dynamic systems can be very complex and strongly sensitive to initial conditions. This situation leads to what is called chaotic behavior. The same complications occur in discrete systems. CAs provide an alternative method to describe, understand, and simulate the behavior of complex systems [40]. A CA model is a dynamic system that is discrete in space and time. The model operates on a uniform, regular lattice of cells. The premise behind a CA model is that a global complex behavior can be simulated by simple local rules that operate on the cells. The solution of simple local equilibrium problems can provide a more accurate and robust procedure to solve large and complex problems. Also, the inherent parallelism of CA models makes this approach very appealing.

A CA model only makes use of local conditions, whereas a HCA model combines local design rules with global structural analysis. The HCA method is intended to solve complex structural optimization problems in engineering. The premise of the HCA approach is that *complex static and dynamic problems can be decomposed into a set of simple local rules that operate on a large number of CAs that only know local conditions*.

A. Components

The HCA model has three components: 1) a lattice of cells, 2) a set of states for each cell, and 3) a set of rules associated with the set of states. The lattice of cells can be defined in an n-dimensional space, but usually the models are incorporated in one, two, or three dimensions. For each automaton in the model, there is a set of J discrete states which can be described as

$$\boldsymbol{\alpha}_i(t) = \begin{Bmatrix} \alpha_i^1(t) \\ \alpha_i^2(t) \\ \vdots \\ \alpha_i^J(t) \end{Bmatrix} \tag{55}$$

and are defined for the discrete location i at the discrete time t. For each state α_i^j there is a corresponding rule R_i^j that defines its evolution in time. This evolution can be expressed as

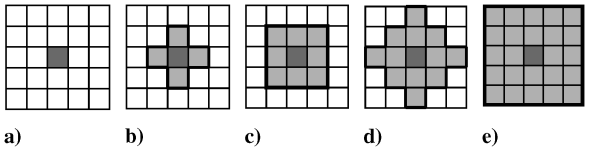

Fig. 1 Neighborhood layouts for a cellular automaton. a) Empty, $\hat{N} = 0$; b) Von Neumann, $\hat{N} = 4$; c) Moore, $\hat{N} = 8$; d) radial, $\hat{N} = 12$; e) extended, $\hat{N} = 24$.

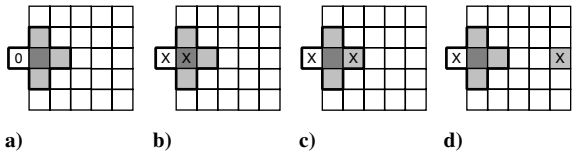

Fig. 2 Boundary conditions for a cellular automaton. a) Fixed; b) adiabatic; c) reflecting; d) periodic.

$$\alpha_i^j(t+1) = R_i^j[\boldsymbol{\alpha}_i(t), \boldsymbol{\alpha}_{i+\Delta_1}(t), \ldots, \boldsymbol{\alpha}_{i+\Delta_{\hat{N}}}(t)] \tag{56}$$

where the $\boldsymbol{\alpha}_{i+\Delta_1}(t), \ldots, \boldsymbol{\alpha}_{i+\Delta_{\hat{N}}}(t)$ designate cells belonging to the neighborhood of the ith cell. That neighborhood is composed of $\hat{N}$ surrounding cells. In the simplest case, a cell has a single state $\alpha_i^1(t)$ that is defined by a single bit of information, $\{0, 1\}$. In the above definition, the set of rules, $\boldsymbol{R}_i = \{R_i^1, \ldots, R_i^J\}^T$, is identical for all sites and is applied simultaneously to all of them which leads to a *synchronous* dynamic. In other words, the rule is *homogeneous*, that is, it does not depend on the position of the cell [40].

In the definition of a local evolutionary rule in Eq. (56), a new state at time $t + 1$ depends on states at time t. It is sometimes necessary to have a lingering memory and introduce a dependence on the states at time $t - 1, t - 2, \ldots, t - T$. Depending on its definition, a rule can be or not be reversible in time.

The set of local rules operates according to local information collected in the neighborhood of each cell. The neighborhood does not have any restriction on size or location, except that it is the same for all the cells. In practice, the size of the neighborhood is often limited to the adjacent cells but can also be extended. Figure 1 depicts some common neighborhood layouts. The most commonly used are the von Neumann layout that includes four neighboring cells ($\hat{N} = 4$) and the Moore layout that includes eight neighboring cells ($\hat{N} = 8$). Another possible layout is the so-called MvonN composed of 12 cells ($\hat{N} = 12$). The neighborhood can also be reduced down to an empty layout ($\hat{N} = 0$) or extended as much as the model requires. In addition to the layouts described above, this work makes use of an extended neighborhood that includes 24 cells ($\hat{N} = 24$).

To define the evolutionary rule for a cell located on the boundary of the design domain, the design domain can be extended in different ways. Figure 2 depicts some types of boundary conditions obtained by extending the design domain. A fixed boundary is defined so that the neighborhood is completed with cells having a preassigned fixed state. An adiabatic boundary condition is obtained by duplicating the value of the cell in an extra virtual neighbor. In a reflecting boundary, the state of the opposite neighbor is replicated by the virtual cell. Periodic boundary conditions are used when the design domain is assumed to be wrapped in a toruslike shape. This work makes use of fixed boundary conditions where the extra cells are considered empty spaces without physical or mechanical properties.

B. Algorithm

The HCA algorithm combines the first-order optimality conditions, the finite element analysis, and the CA components. In the HCA method, the state of the ith cell, $\boldsymbol{\alpha}_i(t)$, is defined by the design variable $x_i(t)$ as described by Eq. (6), and the state variable $y_i(t)$ as described by Eq. (37). This is

$$\boldsymbol{\alpha}_i(t) = \begin{Bmatrix} x_i(t) \\ y_i(t) \end{Bmatrix} \tag{57}$$

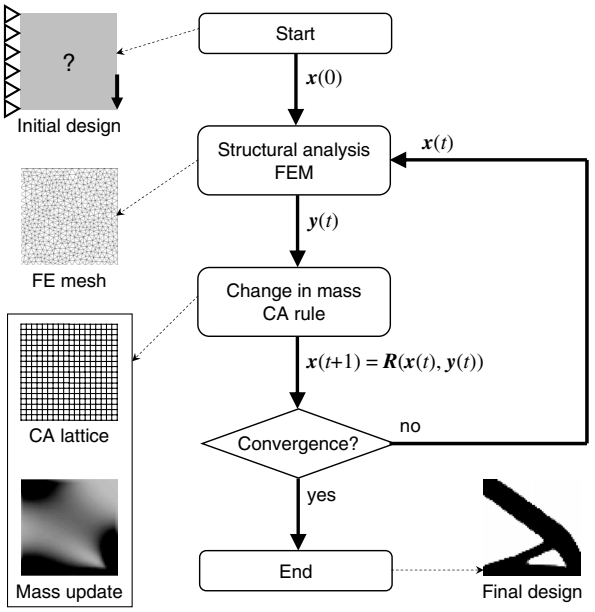

Fig. 3 Hybrid cellular automaton algorithm. The algorithm starts with the definition of the design domain, material properties, load conditions, and initial design $x(0)$. Finite element analysis (FEA) is performed to determine the mechanical stimuli $y(t)$. The mass is updated according to the set of rules, $x(t+1) = R(x(t), y(t))$. The convergence is satisfied when the change in mass is small. If there is no convergence the process continues with a new FEA.

Using fixed boundary conditions, the state of the outer cells in the neighborhoods at the boundaries of the design domain is given by

$$\boldsymbol{\alpha}_k(t) = \begin{Bmatrix} 0 \\ 0 \end{Bmatrix} \tag{58}$$

The HCA algorithm, illustrated in Fig. 3, is described as follows [23]:

Step 1: Define the design domain, lattice of cells, material properties, load conditions, and initial design $x_i(0)$ for each cell.

Step 2: Evaluate the state variable $y_i(t)$, defined by Eq. (37), using the finite element method.

Step 3: Apply the local evolutionary rule R_i and update the mass fraction $x_i(t+1)$ for each cell.

Step 4: Check for convergence. If the structure does not change with respect to the previous designs, the convergence criterion is satisfied, see Eq. (66); otherwise, the iterative process continues from step 2.

In the HCA methodology, the local design rule makes use of an effective value of the design variable, $\bar{x}_i(t)$, and an effective value of the state variable, $\bar{y}_i(t)$ [41]. The effective values are determined as the average value in the neighborhood. This can be expressed as

$$\bar{x}_i(t) = \frac{x_i(t) + \sum_{k=1}^{\hat{N}} x_k(t)}{\hat{N}+1} \tag{59}$$

and

$$\bar{y}_i(t) = \frac{y_i(t) + \sum_{k=1}^{\hat{N}} y_k(t)}{\hat{N}+1} \tag{60}$$

The effective values of the state variables have been used to model cellular communication in biological structures. Similar ideas, using a spatial influence region, have been implemented in bone remodeling simulations [42,43]. In CA-based topology optimization, [25] also makes use of an averaging scheme of the strain energy density for truss structures. In the same way, an effective error $\bar{e}_i(t)$ can be stated as

$$\bar{e}_i(t) = \frac{e_i(t) + \sum_{k=1}^{\hat{N}} e_k(t)}{\hat{N}+1} \tag{61}$$

where $e_i(t)$ is defined in Eq. (52). The local evolutionary rule R_i is determined according to the approaches presented in Sec. IV.

VI. Implementation

To illustrate the implementation of the HCA algorithm, let us consider the topology optimization of a Michell-type two-dimensional structure in a continuum design domain [44]. The design domain has an area of 50×25 mm^2, and its thickness is 1 mm. It is discretized into 50×25 identical cells. One of its lower corners is restrained from vertical and horizontal displacement, while the displacement of the opposite lower corner is constrained only in the vertical direction (Fig. 4). A vertical load of 100 N is applied in the middle of the lower edge. The mechanical properties of the isotropic material comprising the domain correspond to the ones of cortical bone [45]. This work considers a Young's modulus of $E = 20$ GPa and a Poisson's ratio of $\nu = 0.3$. The HCA method was originally developed to predict optimal configurations of the bone internal architecture [41]. The use of the bone elastic (isotropic) properties is merely for illustration purposes.

The optimization problem consists of maximizing the stiffness of the structure while minimizing its mass. As previously stated in Eq. (5), this problem can be expressed as

$$\min_{\boldsymbol{x}} \quad c(\boldsymbol{x}) = \omega \frac{U}{U_0} + (1-\omega)\frac{M}{M_0} \qquad \text{s.t.} \quad \mathbf{0} \le \boldsymbol{x} \le \mathbf{1} \tag{62}$$

The strain energy of the solid structure, U_0, is determined with the finite element method and has a value of $U_0 = 2261$ N $\cdot$ mm. The mass of the solid structure is defined as

$$M_0 = \sum_{i=1}^{N} m_0 = \sum_{i=1}^{N} v_0 \rho_0 \tag{63}$$

In this model, the volume of each cell is $v_0 = 1$ mm^3. Cortical bone density has a value of $\rho_0 = 2.0 \times 10^{-3}$ g/mm^3. Therefore, the total mass of the solid design domain is given by $M_0 = 50 \times 25 \times 2 \times 10^{-3}$ g, which yields $M_0 = 2.5$ g.

The optimum value of the state variable y_i^*, as defined by Eq. (38), can be written as

$$y_i^* = \frac{(1-\omega)}{\omega}\frac{\rho_0 v_0}{p}\frac{U_0}{M_0} \tag{64}$$

Using a penalization power of $p = 3$, and assuming that the cost of the material is 3 times the cost of the strain energy, $\omega = 0.25$, the optimum value of the sate variable can be simplified to $y_i^* = \rho_0 v_0 U_0 / M_0$. Substituting the constants into Eq. (64), the resulting optimum value is $y_i^* = 1.8084$ N $\cdot$ mm/mm^3. The iterative optimization process converges when no further change in mass is possible. This can be stated as

$$\Delta M(t) = M(t) - M(t-1) \approx 0 \tag{65}$$

However, numerical experience with the HCA algorithm has shown that in some applications $\Delta M(t)$ has a cyclic behavior in which a

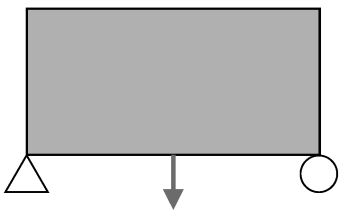

Fig. 4 Michell-type structure. The continuum design domain of $50 \times 25 \times 1$ mm^3 is discretized into 50×25 identical CAs. The isotropic material has a Young's modulus of $E = 20$ GPa and a Poisson's ratio of $\nu = 0.3$. The vertical load applied at the center of the lower edge is 100 N.

small change in mass is followed by a bigger change. To avoid premature convergence, the convergence criterion is defined with the average change in two consecutive iterations. This can be expressed as

$$\frac{|\Delta M(t)| + |\Delta M(t-1)|}{2} \leq \varepsilon \tag{66}$$

where ε is a small fraction of the total mass of the solid structure. In this application, the fraction value is defined as $\varepsilon = 0.001 \times M_0$, which yields $\varepsilon = 2.5 \times 10^{-3}$ g. If there is no convergence after 60 iterations, the iterative process is interrupted and finished. Table 1 summarizes the default parameters of the HCA algorithm for this implementation.

VII. Results

The performance of the HCA algorithm is demonstrated for the two types of design rules developed in this investigation: the ratio technique and the control strategy.

A. Ratio Technique

The ratio technique is a design rule derived from the method traditionally used to solve truss structures under the FSD criterion. The derivation of this approach for continuum structures is demonstrated in Sec. IV.A. The type of neighborhood that defines the effective value of the state variables, $\bar{y}_i(t)$, and the effective value of the design variables, $\bar{x}_i(t)$, has a significant effect on the final topology.

Let us first consider the case in which both the effective state variables and the effective design variables are obtained using the empty neighborhood, $\hat{N} = 0$. In this case, $\bar{x}_i(t) = x_i(t)$ and $\bar{y}_i(t) = y_i(t)$. The algorithm converges in 23 iterations with an objective function value of $c(\boldsymbol{x}) = 0.7455$. Figure 5 shows the final topology and the values of $f(U)$, $g(M)$, and $c(\boldsymbol{x})$ during the iterative process.

In this first case, the final topology suffers from a numerical instability referred to as *checkerboarding*. Checkerboarding describes the regions where solid elements (black) and voids (white) alternate forming a checkerboard pattern. For topology design, the origin of these patterns is related to features of the finite element approximation and, more specifically, to poor numerical modeling that overestimates the stiffness of the checkerboards [30].

Usually, image filtering techniques, gradient constraint, and perimeter control strategies are used to deal with numerical instabilities such as checkerboarding [46,47]. The purpose of these techniques is to smooth the spatial variation in the design variables to avoid instabilities; however, convergence delays and intermediate densities are associated with these techniques.

Let us now consider a second case in which $\bar{x}_i(t)$ is determined using the Moore neighborhood, $\hat{N} = 8$, while $\bar{y}_i(t)$ is determined using the empty neighborhood, $\hat{N} = 0$. This strategy has the effect of using an image filtering technique. Figure 6 depicts the final result which is free of checkerboard patterns. However, in comparison to the first case, the convergence of the algorithm is delayed and achieved only after 45 iterations. Also, the final objective function value worsens to $c(\boldsymbol{x}) = 0.7634$. Additionally, the resulting topology is qualitatively different than the one obtained in the first case. Although the first solution depicts a structure with five interior holes (neglecting the checkerboarding), this structure eliminates two of the radial columns and creates a structure with just three interior holes. These two topologies represent two local minima of the optimization problem.

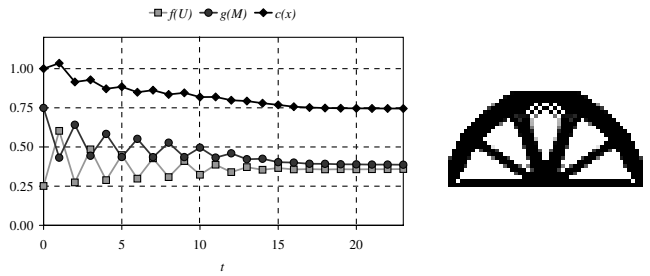

Fig. 5 Topology optimization with the ratio technique—case 1. The empty neighborhood, $\hat{N} = 0$, is used to calculate both the design and the state variable effective values. The final topology is characterized by checkerboard patterns that make that region artificially light and stiff. The design process converged in 23 iterations. The final objective functions have values of $f(U) = 0.3588$, $g(M) = 0.3867$, and $c(\boldsymbol{x}) = 0.7455$.

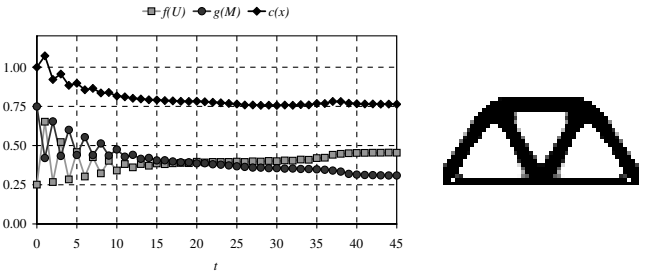

Fig. 6 Topology optimization with the ratio technique—case 2. The Moore neighborhood, $\hat{N} = 8$, is used to calculate $\bar{x}_i(t)$, while $\bar{y}_i(t)$ is determined with the empty neighborhood, $\hat{N} = 0$. The final topology does not have checkerboarding patterns. The design process converged in 45 iterations. The final objective functions have a value of $f(U) = 0.4544$, $g(M) = 0.3091$, and $c(\boldsymbol{x}) = 0.7634$.

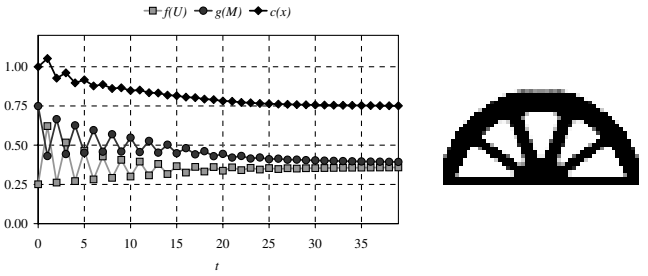

Fig. 7 Topology optimization with the ratio technique—case 3. The Moore neighborhood, $\hat{N} = 8$, is used to calculate $\bar{y}_i(t)$, while $\bar{x}_i(t)$ is determined with the empty neighborhood, $\hat{N} = 0$. The design process converged in 39 iterations. The final objective functions have a value of $f(U) = 0.3581$, $g(M) = 0.3931$, and $c(\boldsymbol{x}) = 0.7511$.

Let us consider a third case in which $\bar{x}_i(t)$ is determined using the empty neighborhood, $\hat{N} = 0$, while $\bar{y}_i(t)$ is determined using the Moore neighborhood, $\hat{N} = 8$. Figure 7 depicts the final topology which is also free of numerical instabilities and qualitatively equivalent to the one obtained in the first case (Fig. 5). In this case, the algorithm converges after 39 iterations with an objective function value of $c(\boldsymbol{x}) = 0.7455$. In comparison to the previous case, the number of iterations is decreased and the value of the objective function is improved.

Finally, let us consider a fourth case in which the Moore neighborhood, $\hat{N} = 8$, is used to evaluate both $\bar{x}_i(t)$ and $\bar{y}_i(t)$. Figure 8 shows the final topology which is qualitatively equivalent to

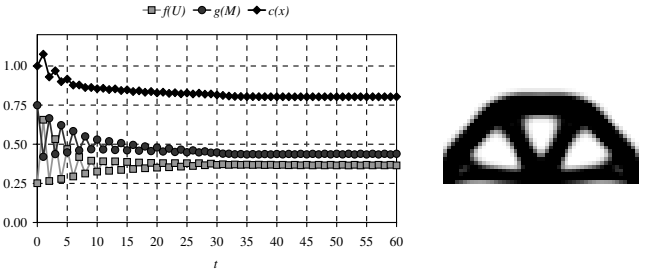

Fig. 8 Topology optimization with the ratio technique—case 4. The Moore neighborhood, $\hat{N} = 8$, is used for both $\bar{x}_i(t)$ and $\bar{y}_i(t)$. A small oscillation prevents the design from convergence before 60 iterations. The values of the objective functions in the last iteration are $f(U) = 0.3645$, $g(M) = 0.4387$, and $c(\boldsymbol{x}) = 0.8033$.

the one obtained in the second case (Fig. 6). In this case, the parameters used in the algorithm impose a design condition that increases the sizes of the resulting trusslike layouts in the final topology. During the iterative process, a small oscillation in the final mass prevents the convergence of the algorithm before 60 iterations.

B. Two-Position Control

The control strategies make use of the effective error signal defined by Eq. (61). The definition of the two-position control is given by Eq. (53). Simplifying the controller with $c_T^F = c_T^R = c_T$, the change in relative density can be expressed as

$$x_i(t+1) = x_i(t) + c_T \times \text{sgn}(\bar{e}_i(t)) \tag{67}$$

where

$$\text{sgn}(\bar{e}_i(t)) = \begin{cases} +1.0 & \text{if } \bar{e}_i(t) > 0 \\ -1.0 & \text{if } \bar{e}_i(t) < 0 \end{cases} \tag{68}$$

The definition of the constant value c_T determines the discrete variation in the relative density of each cell at every iteration. This value also affects the overall behavior of the system. Lower values of c_T, for example, $c_T < 0.05$, delay the convergence of the algorithm, whereas larger values, for example, $c_T > 0.25$, might produce unstable results. Figures 9 and 10 depict the convergence plots for $f(U)$, $g(M)$, and the cost function $c(\boldsymbol{x})$ along with the final topologies for $c_T = 0.10$ and $c_T = 0.25$, respectively.

C. Proportional (P) Control

The proportional (P) control refers to the case in which $c_I = c_D = 0$ in the definition of the PID control given by Eq. (54). With the P control, the change in relative density takes the form

$$x_i(t+1) = x_i(t) + c_P \times \bar{e}_i(t) \tag{69}$$

The selection of the proportional gain c_P affects the convergence during the design process. Let us consider a value of $c_P = 0.20/y_i^*$, in which the equilibrium value y_i^* is used to normalize the effective error $\bar{e}_i(t)$. The result is a slow asymptotic convergence (Fig. 11).

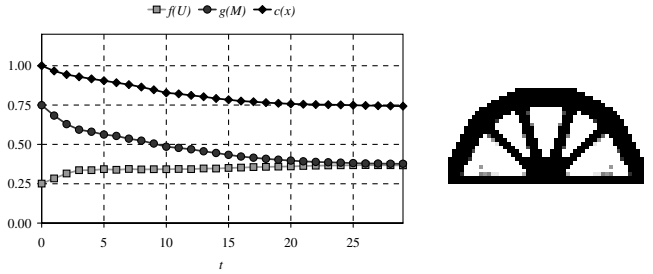

Fig. 9 Topology optimization with two-position control—$c_T = 0.10$. The final topology is obtained after 29 iterations. The values of the objective functions are $f(U) = 0.3664$, $g(M) = 0.3767$, and $c(x) = 0.7431$.

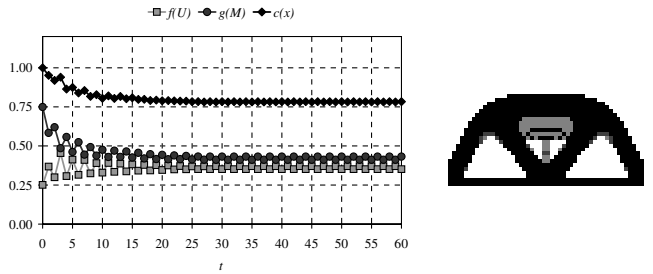

Fig. 10 Topology optimization with two-position control—$c_T = 0.25$. No convergence is achieved before 60 iterations. The values of the objective functions in the last iteration are $f(U) = 0.3515$, $g(M) = 0.4318$, and $c(x) = 0.7833$.

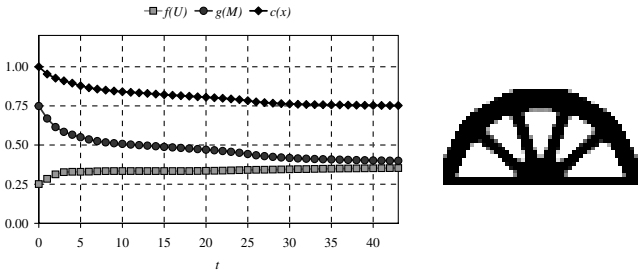

Fig. 11 Topology optimization with P control—$c_P = 0.20/y_i^*$. The final topology is obtained after 43 iterations. The values of the objective functions are $f(U) = 0.35283$, $g(M) = 0.39933$, and $c(x) = 0.7522$.

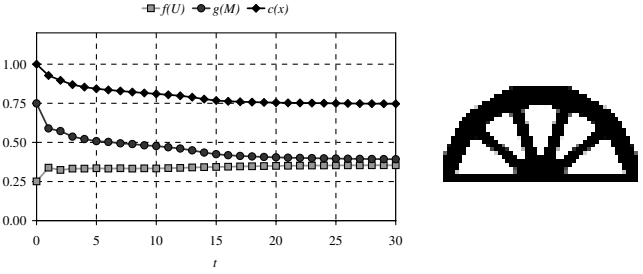

Fig. 12 Topology optimization with P control—$c_P = 0.40/y_i^*$. The final topology is obtained after 30 iterations. The values of the objective functions are $f(U) = 0.3540$, $g(M) = 0.3925$ and $c(x) = 0.7465$.

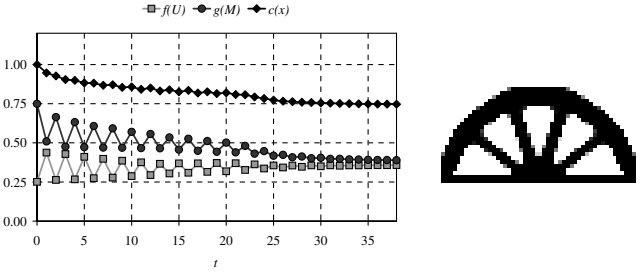

Fig. 13 Topology optimization with P control—$c_P = 0.60/y_i^*$. The final topology is obtained after 38 iterations. The values of the objective functions are $f(U) = 0.3575$, $g(M) = 0.3891$, and $c(x) = 0.7466$.

The increment in the proportional gain to $c_P = 0.40/y_i^*$ reduces the convergence time (Fig. 12); however, further incrementing to $c_P = 0.60/y_i^*$ affects the stability of the system creating oscillations that increase the number of iterations (Fig. 13). These three cases can be compared to the vibratory response of a dynamic system characterized by overdamped, critically damped, and underdamped behavior [48].

D. Proportional-Integral (PI) Control

The proportional-integral (PI) control refers to the case in which $c_D = 0$ in the definition of the PID control given by Eq. (54). With a PI control, the change in density takes the form

$$x_i(t+1) = x_i(t) + c_P \times \bar{e}_i(t) + c_I \times \sum_{\tau=0}^{t} \bar{e}_i(t-\tau) \tag{70}$$

For the initial design at $t = 0$, the state of the previous effective error is defined as $\bar{e}_i(-1) = 0$. A modified approach, not presented here, considers $\bar{e}_i(-1) = \bar{e}_i(0)$. Numerically, this modified approach leads to a prolonged initial response that decreases the stability of the system.

The addition of the integral action improves the steady-state performance of the control algorithm; however, it also might lead to an oscillatory response in the transient state [39]. Let us consider the case in which $c_P = 0.20/y_i^*$ and $c_I = 0.30/y_i^*$. As Fig. 14 illustrates,

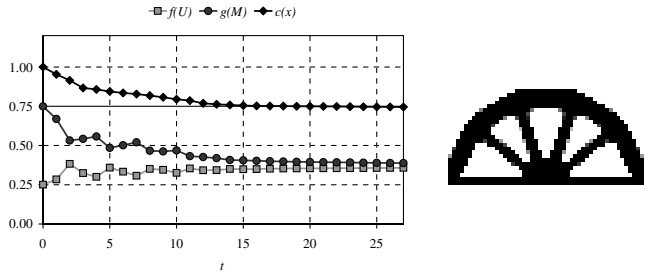

Fig. 14 Topology optimization with PI control—$c_P = 0.20/y_i^*$, $c_I = 0.30/y_i^*$. The final topology is obtained after 27 iterations. The values of the objective functions are $f(U) = 0.3575$, $g(M) = 0.3880$, and $c(x) = 0.7455$.

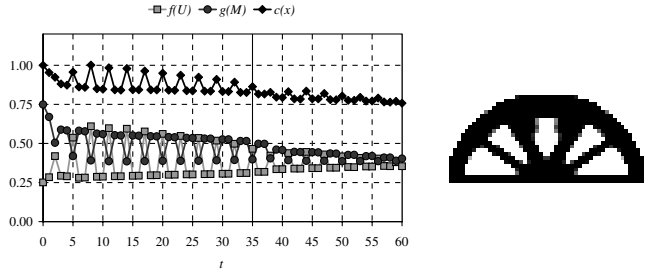

Fig. 15 Topology optimization with PI control—$c_P = 0.20/y_i^*$, $c_I = 0.40/y_i^*$. No convergence is achieved before 60 iterations. The values of the objective functions in the last iteration are $f(U) = 0.3544$, $g(M) = 0.4032$, and $c(x) = 0.7576$.

the convergence is improved with respect to the previous P control (Fig. 11). The response in the transient state is characterized by a rather smooth oscillation. Further increase of the integral gain to $c_I = 0.40/y_i^*$ amplifies the oscillatory response and delays the convergence (Fig. 15).

E. PID Control

The PID control is given by Eq. (54). With the PID control, the change in density takes the form

$$x_i(t+1) = x_i(t) + c_P \times \bar{e}_i(t) + c_I \times \sum_{\tau=0}^{t} \bar{e}_i(t-\tau) + c_D \times [\bar{e}_i(t) - \bar{e}_i(t-1)] \tag{71}$$

For the initial design at $t = 0$, the state of the previous effective error is defined as $\bar{e}_i(-1) = 0$ for the integral action; however, the selection of $\bar{e}_i(-1) = \bar{e}_i(0)$ is preferred for the derivative action. In this way, the initial response is not amplified and the stability of the system is improved.

The stability of the system can be improved by adding a derivative action to the control algorithm. The derivative controller provides an anticipatory effect that results in a damping of the system response during the transient state. In this way, it becomes possible to use a greater loop gain, thus providing speed of response and reducing steady-state error [39].

The effect of the PID controller is demonstrated by adding the derivative action to the previous PI case. For the control gains $c_P = 0.20/y_i^*$, $c_I = 0.40/y_i^*$, and $c_D = 0.20/y_i^*$, the convergence in the design process is improved. In comparison to the the PI response (Fig. 15), the PID action dampens the oscillation in the transient state and the optimum topology is reached in fewer iterations (Fig. 16.)

Defining the optimal adjustment of these control gains is one of the basic problems faced by control engineers. The tuning rules [49] or self-tuning methods [50] can provide some procedures for this purpose. In this preliminary study the values are set based on numerical experimentation.

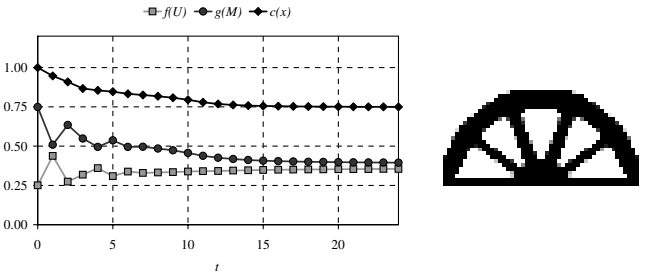

Fig. 16 Topology optimization with PID control—$c_P = 0.20/y_i^*$, $c_I = 0.40/y_i^*$, and $c_D = 0.20/y_i^*$. The final topology is obtained after 16 iterations. The values of the objective functions are $f(U) = 0.3549$, $g(M) = 0.3926$, and $c(x) = 0.7475$.

a) b) c)

Fig. 17 Topologies of different Pareto points. a) $\omega = 0.05$, $c(x) = 0.4396$. b) $\omega = 0.25$, $c(x) = 0.7465$. c) $\omega = 0.50$, $c(x) = 0.9393$.

F. Pareto Optimality

The structural optimization problem in Eq. (5) considers two conflicting objectives: minimizing strain energy U and minimizing mass M. This problem has an infinite number of solutions depending on the selection of the weight coefficient ω. Each solution is denoted as a Pareto optimum. The set of all Pareto optima forms the Pareto front. The Pareto front provides an insight into the optimization problem that cannot be obtained by looking at a single point in the design space.

The complete Pareto front can be obtained by varying the weight coefficient ω from 0 to 1. This coefficient determines the optimum value of the state variable y_i^* according to Eq. (38) and, therefore, the final topology. Figure 17 shows the final topologies corresponding to $\omega = 0.05$, $\omega = 0.25$, and $\omega = 0.50$. Final designs are plotted as Pareto points in the space of objective functions (Fig. 18).

G. Comparison

For comparison, let us consider the optimality criterion OC-SIMP heuristic updating scheme proposed by Bendsøe [51] and implemented in MATLAB by Sigmund [29]. The objective problem in that approach is to minimize compliance subject to a volume constraint. A mesh-independency filter works by modifying the element sensitivities.

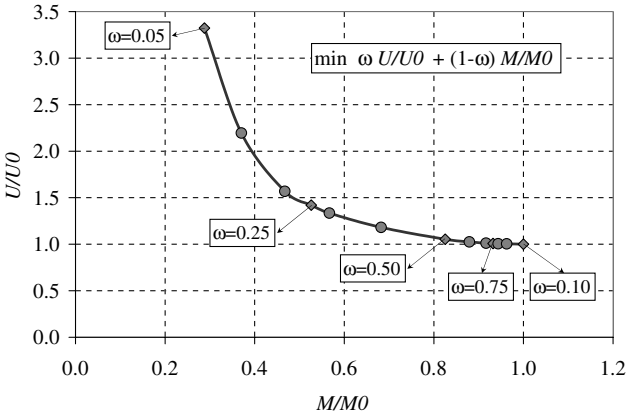

Fig. 18 The set of all Pareto optima forms the Pareto front that is shown as a curve in the space defined by the relative final strain energy U/U_0 and the relative final mass M/M_0. The Pareto front is limited on the right-hand side by $\omega = 1$, for which $M/M_0 = 1$ and $U/U_0 = 1$, and limited on the left-hand side by $\omega = 0$, for which $M/M_0 = 0$ and $U/U_0 = \infty$.

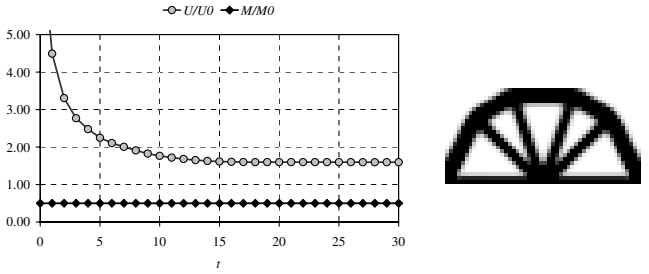

Fig. 19 Topology optimization using Sigmund's MATLAB code [29]. The plot shows the first 30 iterations. The mass constraint is $M/M_0 = 0.5$. The final value of the objective function is $U/U_0 = 1.5898$, which corresponds to $f(U) = 0.3975, g(M) = 0.3750$, and $c(x) = 0.7725$.

To provide a comparison, the objective problem was modified to minimize a normalized strain energy, U/U_0, subject to a normalized mass constraint, $M/M_0 = 0.5$. In this way, the final value of the mass function, $g(M) = (1 - \omega)M/M_0$, would be similar to the ones obtained using the HCA method for $\omega = 0.25$, $g(M) = (0.75)(0.5) = 0.375$. Figure 19 shows the convergence and final topology.

VIII. Conclusions and Final Remarks

The HCA method presented in this investigation is a new approach to topology optimization for continuum structures. This non-gradient-based method makes use of the finite element method for structural analysis and the cellular automaton paradigm to apply local evolutionary rules. The HCA follows optimization principles derived from the KKT conditions. The contribution of this paper is the explicit form of the KKT conditions and their application to the local evolutionary rules.

The HCA method is not a mathematical programming technique that solves equations like Eqs. (5) or (62), but is instead a methodology that synthesizes a structure that satisfies the optimality conditions for those problems using cellular automata. Original methodologies developed in this research, which are based on the ratio technique and control strategies, drive the structure to an optimal configuration. The ratio technique developed in this research is specifically developed to synthesize a continuum structure that satisfies the optimality conditions of a particular multi-objective structural optimization problem, that is, minimizing both mass and strain energy. The control strategies allow one to modify parameters that could potentially decrease the number of iterations. The density approach is used as the material model; however, the HCA algorithm can be extended to other material models, for example, microstructural models.

In the HCA method, the design domain is discretized into a regular lattice of cells that may be independent of the finite element mesh. The convergence in this method is determined by local evolutionary rules. The rules modify the design variables to achieve the zero-error condition between the effective value of the state variables and their optimum value. The effective value of the state variable is defined as the average value in the neighborhood of the cell. The state variable and its optimum value are derived from the KKT conditions of the structural optimization problem to be solved. This investigation develops the corresponding expressions from the multi-objective optimization problem that minimizes both strain energy and mass.

In the HCA method, the local equilibrium condition shares similarities with the FSD approach. The optimality criterion implies that a cell that is not void is fully stressed. Based on a traditional ratio technique used to optimize truss structures under the FSD approach, this investigation develops a new set of rules that are suitable for continuum structures under the parameters of the HCA algorithm. The monotonicity between the design variable and the state variable makes possible the use of local design rules based on control theory. This condition also avoids the use of sensitivity analysis during the design process. The extension of the HCA methods to problems where this monotonicity no longer exists is under development.

This work demonstrates the implementation and performance of the HCA algorithm through a two-dimensional sample problem. It also illustrates the influence of different parameters applied to the evolutionary rules. There are many local minima in the topology optimization problem solved in this investigation. A change in the HCA parameters leads to qualitatively different solutions or local minima.

In topology optimization, approaches that make use of the spatial variation of state variables have not been as widely explored as the ones related to image filtering, that is, a weighted average of design variables. This investigation demonstrates the effect of averaging both design variables and state variables. The HCA method does not require the use of image filtering techniques, gradient constraint, or perimeter control strategies to prevent numerical instabilities such as checkerboarding. The computational efficiency of the iterative process is given by the type of evolutionary rule applied.

The local design rules based on control theory make use of the two-position and PID action. The PID control requires tuning of the proportional, integral, and derivative gains. A wrong selection of the gain values might decrease the stability margins of the convergence. In the ratio technique, no gains need to be adjusted. In this sense, this technique is simpler to implement; however, the convergence might take longer in comparison to the PID control rules. Current research is implementing the HCA method to solve other optimization problems such as minimizing mass subject to stress and displacement constraints.

Acknowledgments

Support for this research has been provided by the Division for Research of the National University of Colombia—División de Investigación, Sede Bogotá, and the Honda Initiation Grant HIG 2005.

References

[1] Bendsøe, M. P., and Kikuchi, N., "Generating Optimal Topologies in Optimal Design Using a Homogenization Method," *Computer Methods in Applied Mechanics and Engineering*, Vol. 71, No. 2, Nov. 1988, pp. 197–224.

[2] Theocaris, P. S., and Stavroulakis, G. E., "Optimal Material Design in Composites: An Iterative Approach Based on Homogenized Cells," *Computer Methods in Applied Mechanics and Engineering*, Vol. 169, Nos. 1–2, Jan. 1999, pp. 31–42.

[3] Allaire, G., *Shape Optimization by the Homogenization Method*," Applied Mathematical Sciences, Vol. 146, Springer, New York, 2002.

[4] Bendsøe, M. P., "Optimal Shape Design as a Material Distribution Problem," *Structural Optimization*, Vol. 1, No. 4, Dec. 1989, pp. 193–202.

[5] Zhou, M., and Rozvany, G. I. N., "The COC Algorithm, Part 2: Topological, Geometry and Generalized Shape Optimization," *Computer Methods in Applied Mechanics and Engineering*, Vol. 89, Nos. 1–3, Aug. 1991, pp. 197–224.

[6] Rozvany, G. I. N., "Aims, Scope, Methods, History and Unified Terminology of Computer-Aided Topology Optimization in Structural Mechanics," *Structural and Multidisciplinary Optimization*, Vol. 21, No. 2, 2001, pp. 90–108.

[7] Schmit, L. A., and Farsi, B., "Some Approximation Concepts for Structural Synthesis," *AIAA Journal*, Vol. 12, No. 5, 1974, pp. 692–699.

[8] Schmit, L. A., and Miura, H., "Approximation Concepts for Efficient Structural Synthesis," NASA CR-2552, March 1976.

[9] Vanderplaats, G. N., and Salajegheh, E., "A New Approximation Method for Stress Constraints in Structural Synthesis," *AIAA Journal*, Vol. 27, No. 3, 1989, pp. 352–358.

[10] Svanberg, K., "The Method of Moving Asymptotes—A New Method for Structural Optimization," *International Journal for Numerical Methods in Engineering*, Vol. 24, No. 2, Feb. 1987, pp. 359–373.

[11] Venkayya, V. B., "Optimality Criteria: A Basis for Multidisciplinary Design Optimization," *Computational Mechanics*, Vol. 5, No. 1, Jan. 1989, pp. 1–21.

[12] Rozvany, G. I. N., Zhou, M., and Gollub, W., "Continuum-Type Optimality Criteria Methods for Large Finite-Element Systems with a Displacement Constraint," *Structural Optimization*, Vol. 2, No. 2, 1990, pp. 77–104.

[13] Saxena, A., and Ananthasuresh, G. K., "On an Optimal Property of Compliant Topologies," *Structural and Multidisciplinary Optimization*, Vol. 19, No. 1, March 2000, pp. 36–49.
[14] Fanjoy, D., and Crossley, W., "Using a Genetic Algorithm to Design Beam Cross-Sectional Topology for Bending, Torsion, and Combined Loading," *Structural Dynamics and Material Conference and Exhibit*, AIAA, Reston, VA, April 2000, pp. 1–9.
[15] Jakiela, M. J., Chapman, C., Duda, J., Adewuya, A., and Saitou, K., "Continuum Structural Topology Design with Genetic Algorithms," *Computer Methods in Applied Mechanics and Engineering*, Vol. 186, Nos. 2–4, June 2000, pp. 339–356.
[16] Xie, Y. M., and Steven, G. P., *Evolutionary Structural Optimization*, Springer, New York, 1993.
[17] Xie, Y. M., and Steven, G. P., "A Simple Evolutionary Procedure for Structural Optimization," *Computers and Structures*, Vol. 49, No. 5, 1993, pp. 885–896.
[18] Inou, N., Uesugi, T., Iwasaki, A., and Ujihashi, S., "Self-Organization of Mechanical Structure by Cellular Automata," *Fracture and Strength of Solids*, Vol. 145, No. 9, 1998, pp. 1115–1120.
[19] Kita, E., and Toyoda, T., "Structural Design Using Cellular Automata," *Structural and Multidisciplinary Optimization*, Vol. 19, No. 1, March 2000, pp. 64–73.
[20] Tatting, B., and Gürdal, Z., "Cellular Automata for Design of Two-Dimensional Continuum Structures," *Proceedings of the 8th AIAA/USAF/NASA/ISSMO Symposium on Multidisciplinary Analysis and Optimization*, AIAA, Reston, VA, 2000.
[21] Hajela, P., and Kim, B., "On the Use of Energy Minimization for CA Based Analysis In Elasticity," *Structural and Multidisciplinary Optimization*, Vol. 23, No. 1, Dec. 2001, pp. 24–33.
[22] Abdalla, M. M., and Gürdal, Z., "Structural Design Using Cellular Automata for Eigenvalue Problems," *Structural and Multidisciplinary Optimization*, Vol. 26, No. 3, 2004, pp. 200–208.
[23] Tovar, A., Niebur, G. L., Sen, M., and Renaud, J. E., "Bone Structure Adaptation as a Cellular Automaton Optimization Process," *Proceedings of the 45th AIAA/ASME/ASCE/AHS/ASC Structures, Structural Dynamics & Materials Conference*, AIAA, Reston, VA, April 2004.
[24] Inou, N., Shimotai, N., and Uesigi, T., "A Cellular Automaton Generating Topological Structures," *Proceedings of the Second European Conference on Smart Structures and Materials*, International Society for Optical Engineering (SPIE), Washington, D.C., 1994, pp. 47–50.
[25] Abdalla, M. M., and Gürdal, Z., "Structural Design Using Optimality Based Cellular Automata," *Proceedings of the 43rd AIAA/ASME/ASCE/AHS/ASC Structures, Structural Dynamics, and Materials Conference*, AIAA, Reston, VA, 2002.
[26] Slotta, D. J., Tatting, B., Watson, L. T., Gürdal, Z., and Missoum, S., "Convergence Analysis for Cellular Automata Applied to Truss Structures," *Engineering Computations*, Vol. 19, No. 8, 2002, pp. 953–969.
[27] Missoum, S., Gürdal, Z., and Setoodeh, S., "Study of a New Local Update Scheme for Cellular Automata In Structural Design," *Structural and Multidisciplinary Optimization*, Vol. 29, No. 2, 2005, pp. 103–112.
[28] Kim, S., Abdalla, M. M., Gürdal, Z., and Jones, M., "Multigrid Accelerated Cellular Automata for Structural Design Optimization: A 1-D Implementation," *Proceedings of the 45th AIAA/ASME/ASCE/AHS/ASC Structures, Structural Dynamics & Materials Conference*, AIAA, Reston, VA, 2004.
[29] Sigmund, O., "A 99 Line Topology Optimization Code Written in Matlab," *Structural and Multidisciplinary Optimization*, Vol. 21, No. 2, April 2001, pp. 120–127.
[30] Bendsøe, M. P., and Sigmund, O., *Topology Optimization Theory, Method and Applications*, Springer, New York, 2003.
[31] Bendsøe, M. P., and Sigmund, O., "Material Interpolations in Topology Optimization," *Archive of Applied Mechanics*, Vol. 69, Nos. 9–10, Nov. 1999, pp. 635–654.
[32] Zienkiewicz, O. C., and Taylor, R. L., *The Finite Element Method*, Vol. 1, The Basis, 5th ed., Butterworth–Heinemann, Stoneham, MA, 2000.
[33] Kwon, Y. W., and Bang, H., *The Finite Element Method Using Matlab*, CRC Press, Boca Raton, FL, 2000.
[34] Haftka, R. T., Gürdal, Z., and Kamat, M. P., *Elements of Structural Optimization*, 2nd ed., Kluwer Academic Publishers, Dordrecht, The Netherlands, 1990.
[35] Tovar, A., "Optimización Topológica con la Técnica de los Autómatas Celulares Híbridos," *Revista Internacional de Métodos Numéricos para Cálculo y Diseño en Ingeniería*, Vol. 21, No. 4, 2005, pp. 365–383.
[36] Huiskes, R., Weinans, H., Grootenboer, J., Dalstra, M., Fudala, M., and Slooff, T. J., "Adaptive Bone Remodelling Theory Applied to Prosthetic-Design Analysis," *Journal of Biomechanics*, Vol. 20, Nos. 11–12, 1987, pp. 1135–1150.
[37] Carter, D. R., "Mechanical Loading History and Skeletal Biology," *Journal of Biomechanics*, Vol. 20, Nos. 11–12, 1987, pp. 1095–1105.
[38] Tovar, A., Patel, N. M., Niebur, G. L., Sen, M., and Renaud, J. E., "Topology Optimization Using a Hybrid Cellular Automaton Approach with Distributed Control," *ASME Journal of Mechanical Design* (to be published).
[39] Shearer, J. L., Kulakowski, B. T., and Gardner, J. F., *Dynamic Modeling and Control of Engineering Systems*, 2nd ed., Prentice–Hall, Upper Saddle River, NJ, 1997.
[40] Chopard, B., and Droz, M., *Cellular Automata Modeling of Physical Systems*, Cambridge Univ. Press, Cambridge, England, U.K., 1998.
[41] Tovar, A., "Bone Remodeling as a Hybrid Cellular Automaton Optimization Process," Ph.D. thesis, University of Notre Dame, IN, 2004.
[42] Mullender, M. G., Huiskes, R., and Weinans, H., "A Physiological Approach to the Simulation of Bone Remodeling as a Self-Organizational Control Process," *Journal of Biomechanical Engineering*, Vol. 27, No. 11, 1994, pp. 1389–1394.
[43] Mullender, M. G., and Huiskes, R., "Proposal for the Regulatory Mechanism of Wolff's Law," *Journal of Orthopaedic Research*, Vol. 13, No. 4, 1995, pp. 503–512.
[44] Michell, A., "The Limits of Economy of Material in Frame-Structures," *Philosophical Magazine*, Vol. 8, No. 47, 1904, pp. 589–597.
[45] Nigg, B. M., and Herzog, W. (eds.), "*Biomechanics of the Musculo-Skeletal System*," Biological Materials, 2nd ed., Wiley, New York, 1999, pp. 49–243.
[46] Sigmund, O., and Petersson, J., "Numerical Instabilities in Topology Optimization: A Survey on Procedures Dealing with Checkerboards, Mesh-Dependencies and Local Minima," *Structural Optimization*, Vol. 16, No. 1, 1998, pp. 68–75.
[47] Cardoso, E. L. and Fonseca, J. S. O., "Complexity Control in the Topology Optimization of Continuum Structures," *Journal of the Brazilian Society of Mechanical Science & Engineering*, Vol. 25, No. 3, 2003, pp. 293–301.
[48] Meirovitch, L., *Elements of Vibration Analysis*, McGraw–Hill, New York, 1986.
[49] Ziegler, G., and Nichols, N. B., "Optimum Settings for Automatic Controllers," *Transactions of the American Society of Mechanical Engineers*, Vol. 64, Nov. 1942, pp. 759–768.
[50] Åström, K. J., and Björn, W., *Adaptive Control*, Addison–Wesley, Reading, MA, 1989.
[51] Bendsøe, M. P., *Optimization of Structural Topology, Shape and Material*, Springer, New York, 1995.

A. Messac
Associate Editor